



Article

Cite this article: Abib N et al. (2023). Persistent overcut regions dominate the terminus morphology of a rapidly melting tidewater glacier. *Annals of Glaciology* **64**(90), 1–12. <https://doi.org/10.1017/aog.2023.38>

Received: 28 November 2022

Revised: 17 March 2023

Accepted: 25 April 2023

First published online: 29 May 2023

Keywords:







Glacier ablation phenomena; ice/ocean interactions; iceberg calving

Corresponding author:

Nicole Abib;

Email: nabib@uoregon.edu

Persistent overcut regions dominate the terminus morphology of a rapidly melting tidewater glacier

Nicole Abib¹ , David A. Sutherland¹ , Jason M. Amundson², Dan Duncan³, Emily F. Eidam⁴, Rebecca H. Jackson⁵, Christian Kienholz² , Mathieu Morlighem⁶ , Roman J. Motyka⁷ , Jonathan D. Nash⁴, Bridget Ovall⁵ and Erin C. Pettit⁴ 

¹Department of Earth Sciences, University of Oregon, Eugene, OR, USA; ²Department of Natural Sciences, University of Alaska Southeast, Juneau, AK, USA; ³Institute for Geophysics, University of Texas at Austin, Austin, TX, USA; ⁴College of Earth, Ocean, and Atmospheric Sciences, Oregon State University, Corvallis, OR, USA; ⁵Department of Marine and Coastal Sciences, Rutgers University, New Brunswick, NJ, USA; ⁶Department of Earth Sciences, Dartmouth College, Hanover, NH, USA and ⁷Geophysical Institute, University of Alaska Fairbanks, Fairbanks, AK, USA

Abstract

Frontal ablation, the combination of submarine melting and iceberg calving, changes the geometry of a glacier's terminus, influencing glacier dynamics, the fate of upwelling plumes and the distribution of submarine meltwater input into the ocean. Directly observing frontal ablation and terminus morphology below the waterline is difficult, however, limiting our understanding of these coupled ice–ocean processes. To investigate the evolution of a tidewater glacier's submarine terminus, we combine 3-D multibeam point clouds of the subsurface ice face at LeConte Glacier, Alaska, with concurrent observations of environmental conditions during three field campaigns between 2016 and 2018. We observe terminus morphology that was predominately overcut (52% in August 2016, 63% in May 2017 and 74% in September 2018), accompanied by high multibeam sonar-derived melt rates (4.84 m d^{-1} in 2016, 1.13 m d^{-1} in 2017 and 1.85 m d^{-1} in 2018). We find that periods of high subglacial discharge lead to localized undercut discharge outlets, but adjacent to these outlets the terminus maintains significantly overcut geometry, with an ice ramp that protrudes 75 m into the fjord in 2017 and 125 m in 2018. Our data challenge the assumption that tidewater glacier termini are largely undercut during periods of high submarine melting.

Introduction

Ice loss from tidewater glaciers worldwide has accelerated in recent decades (e.g. Mouginot and others, 2019) due to a decrease in surface mass balance and an increase in ice discharge to the ocean (e.g. Enderlin and others, 2014; Van Den Broeke and others, 2016). A primary driver of increased mass loss into the ocean has been oceanic warming, through its influence on glacier frontal ablation, which is the combination of iceberg calving and submarine melting (Motyka and others, 2003; Holland and others, 2008; Howat and others, 2008; Straneo and others, 2013; Wood and others, 2018; Kochtitzky and others, 2022). Frontal ablation changes the geometry of a glacier's terminus, and can influence glacier dynamics by reduced resistance to glacier flow (Podrasky and others, 2014) through detachment from pinning points in the fjord (Benn and others, 2007) and retreat from a stable grounding line (Catania and others, 2018). Changes in terminus geometry can also impact the upwelling of subglacial discharge plumes (Jenkins, 2011; Slater and others, 2017), thereby altering near-glacier ocean currents that affect submarine melt rates and creating a complex feedback loop between glacier change and ocean circulation. While the feedbacks between ocean properties and glacier change have been recognized as important, process-based understanding of this relationship is still underdeveloped, largely due to the lack of observational data close to tidewater glacier termini.

The timing and magnitude of changes in tidewater glacier geometry are controlled by two processes: iceberg calving and submarine melting. Iceberg calving events occur due to brittle failure of ice, causing rapid and jagged changes in shape (Benn and others, 2007; Fried and others, 2019). On the contrary, submarine melting is thought to depend on the velocity and temperature of the ocean near the ice–ocean interface, resulting in more gradual changes to glacier terminus geometry (Holland and Jenkins, 1999; Jenkins, 1999; Fried and others, 2019). Based on the assumption that submarine melt scales with water velocity adjacent to the ice, melt rates near the location of upwelling subglacial discharge plumes are thought to be higher than those away from discharge outlets (Cowton and others, 2015; Slater and others, 2015; Carroll and others, 2016). Recent work, however, has shown that submarine melt rates can be up to two orders of magnitude higher than those predicted by plume-melt theory (Sutherland and others, 2019; Jackson and others, 2020, 2022), which describes the coupling of buoyant plume theory with a three-equation melt parameterization (Holland and Jenkins,

© The Author(s), 2023. Published by Cambridge University Press on behalf of International Glaciological Society. This is an Open Access article, distributed under the terms of the Creative Commons Attribution licence (<http://creativecommons.org/licenses/by/4.0/>), which permits unrestricted re-use, distribution and reproduction, provided the original article is properly cited.

[cambridge.org/aog](https://www.cambridge.org/aog)



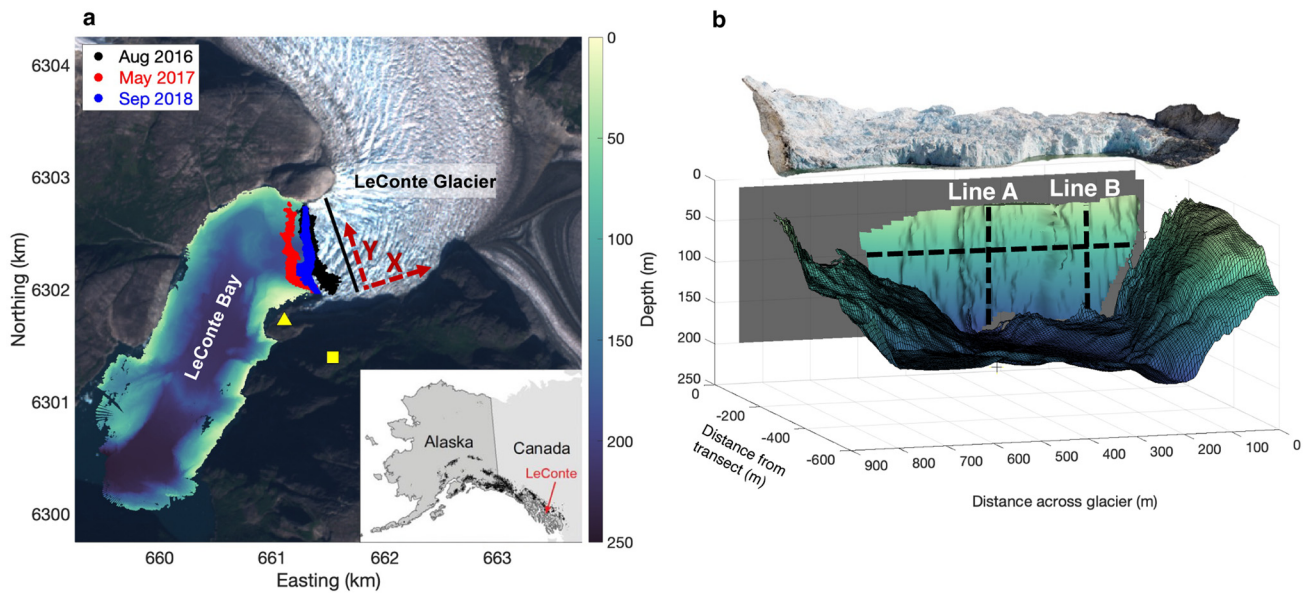


Figure 1. Study area. (a) Sentinel 2-A image of LeConte Glacier and Bay in September 2018 with markers indicating the location of the TRI and the upper time-lapse cameras (yellow square), the lower time-lapse cameras (yellow triangle), as well as the collected multibeam point clouds (black: August 2016, red: May 2017, blue: September 2018). An example reference transect (black line) and rotated coordinate system (red dashed lines) is shown overtop the glacier. Map is referenced to UTM Zone 8N and the inset shows location of LeConte Glacier in southeast Alaska. (b) Example output from multibeam sonar showing the subaerial and submarine terminus geometry, gridded bathymetry and reference plane used for projection and gridding of the point clouds (grey rectangle). Image of the subaerial terminus was acquired from UAV imagery and manually lined up with the submarine terminus. Dashed lines correspond with the transects taken for panels a-c in Figure 2, and all vertical transects are shown in a Supplementary video.

1999; Jenkins, 2011; Cowton and others, 2015), particularly away from the direct influence of discharge plumes.

Although often considered separately, submarine melting can influence iceberg calving through changes to the geometry of the submarine terminus. Several studies have suggested that submarine melting alters the stress state in the near-terminus region, exerting a first-order control on the calving regime of tidewater glaciers (e.g. O’Leary and Christoffersen, 2013; Benn and others, 2017; Cowton and others, 2019; Ma and Bassis, 2019; Slater and others, 2021). When iceberg calving rates are larger than they would be in the absence of submarine melting, this is referred to as a ‘calving multiplier’ (O’Leary and Christoffersen, 2013; How and others, 2019; Ma and Bassis, 2019). In glacier evolution models, iceberg calving events are typically parameterized based on ice thickness, grounding line depth, ice stresses and glacier velocities (Amaral and others, 2020). The dearth of temporally evolving 3-D terminus geometries has made validation of these models difficult (Ma and Bassis, 2019); therefore, prior investigations into ‘calving multipliers’ have relied on idealized submarine terminus morphologies, typically either undercut or assuming a vertical calving face. A growing body of evidence suggests the presence of various overcut morphologies, including underwater ice ramps (Hunter and Powell, 1998; Motyka and others, 1998; Rignot and others, 2015; Wagner and others, 2016, 2019; Mercenier and others, 2019, 2020), terraces (Sugiyama and others, 2019) or grounding line toes (Fried and others, 2019), for which the influence on near-terminus stresses is largely uninvestigated. Understanding the 3-D geometry and evolution of the subsurface terminus is therefore essential for predicting feedbacks between ocean-driven melting and near-terminus glacier dynamics.

Directly observing time-varying terminus geometry is challenging due to hazardous field conditions near the front of tidewater glaciers. A handful of studies have used multibeam sonar in Alaska (Sutherland and others, 2019) and Greenland (Fried and others, 2015, 2019; Rignot and others, 2015; Wagner and others, 2019) to map the terminus beneath the waterline in 3-D space. These surveys show heterogeneous morphology across the width of the terminus, with evidence of large undercut regions present

at the location of subglacial discharge plumes and more vertical terminus slopes away from these discharge outlets (Fried and others, 2015, 2019; Rignot and others, 2015). Such variations in terminus morphology are unlikely to be driven by glacier flow, which is often dominated by sliding near the terminus and typically assumed to be nearly spatially uniform from the bed to the surface. This suggests that these varying morphologies result from different frontal ablation processes across the width and depth of a glacier’s terminus: melting by deep, warm water drawn in by subglacial discharge at depth (Rignot and others, 2015; Fried and others, 2019) can produce undercutting, calving in the upper water column (Fried and others, 2019) would produce overcutting and ocean-driven ambient melting away from the discharge plume (Sutherland and others, 2019; Wagner and others, 2019) may create differing local geometries. Each of these surveys, however, is limited to one point in time, preventing us from investigating the evolution of the submarine terminus and understanding the relationship between local environmental forcings, terminus geometry and glacier dynamics.

Here we use a novel dataset from LeConte Glacier (Xeitol Sít’ in Tlingit), Alaska, to investigate the temporal evolution of the subsurface terminus and relate it to the spatial patterns and drivers of frontal ablation. We combine high-resolution maps of the glacier’s submarine terminus from repeat multibeam sonar imaging with concurrent observations of subaerial geometry derived from terrestrial radar interferometry and time-lapse imagery collected during three field campaigns between 2016 and 2018. Our results provide the first concurrent observations of time-varying 3-D terminus geometry and environmental forcings, allowing us to investigate the evolution of the submarine terminus across a wide parameter space of environmental conditions.

Physical setting

LeConte Glacier is a fast-flowing ($15\text{--}25\text{ m d}^{-1}$) tidewater glacier that terminates in LeConte Bay (Xeitol Geeyi’ in Tlingit), $\sim 30\text{ km}$ from Petersburg in southeast Alaska (Fig. 1a; O’Neil and others, 2001). With a terminus width of $\sim 1\text{ km}$ and a maximum

grounding line depth of 200 m (Sutherland and others, 2019), the dimensions of LeConte Glacier make it a relatively accessible analog for smaller outlet glaciers around the periphery of the Greenland ice sheet. In addition, the springtime oceanic temperature and water column stratification at LeConte Glacier are similar to typical conditions observed in Greenlandic proglacial fjords (Jackson and others, 2022). Throughout the year, the glacial system is exposed to a range of ocean temperatures (4–7°C at depth; Hager and others, 2022) and subglacial discharge (20–350 m³ s⁻¹; Amundson and others, 2020), with outflowing plumes (Motyka and others, 2003) and a recirculation gyre (Kienholz and others, 2019) typically visible in the near-terminus surface waters. Several prior studies at LeConte Glacier using a combination of ocean observations both further from (~1.5 km away; Motyka and others, 2003, 2013; Jackson and others, 2022) and near the glacier terminus (~350 m away; Jackson and others, 2020), as well as multibeam sonar (Sutherland and others, 2019), found very high rates of ocean-driven melting at the glacier (up to 15 m d⁻¹), accounting for up to 50% of the total ice flux to the terminus in the summer months. Additional near-terminus autonomous kayak surveys revealed the ubiquitous presence of ambient meltwater intrusions into the proglacial fjord, suggesting elevated rates of submarine melting even several hundred meters from the upwelling subglacial discharge plume (Jackson and others, 2020).

Methods

Submarine glacier morphology

We surveyed the glacier terminus and proglacial bathymetry using a Reson SeaBat 7111 multibeam echosounder and Applanix POS/MV 320 Wave Master in August 2016 and a Reson SeaBat T50-P multibeam system in May 2017 and September 2018 to investigate the 3-D geometry and evolution of the submarine terminus (Fig. 1b). We inserted a 15° wedge into the multibeam system to enable scanning of the grounding line and the submarine ice face at a distance of ~300 m from the terminus following the methods of Sutherland and others (2019). This side-scanning multibeam sonar produces a 3-D point cloud from the fjord floor to ~20 m below the fjord's surface. We determined the grounding line by using a break in the slope of the point cloud (Sutherland and others, 2019; Eidam and others, 2020). Scans of the terminus collected within 1 h of each other were combined so that each scan then represented a single trip to the ice face and covered as much of the submarine terminus as possible. This resulted in six near-complete terminus scans between 9 and 15 August 2016, five scans between 10 and 12 May 2017 and 13 scans between 13 and 18 September 2018. To assess the error of these point clouds, we compared the data over two patches of bedrock (~15 000–17 000 m²) near the terminus, finding maximum errors of 5.3 m in August 2016, 2.6 m in May 2017 and 2.4 m in September 2018 (Sutherland and others, 2019; Eidam and others, 2020).

Next, we defined a 2-D reference plane up-glacier from the terminus and perpendicular to ice flow onto which we projected and gridded the point clouds at resolutions of 5–20 m to account for uncertainty in our projection of a 3-D point cloud onto a 2-D plane (Fig. 1b; Sutherland and others, 2019). For the gridded scans, we calculated the vertical and horizontal slopes of the terminus for each gridcell. These slopes were then smoothed with a box filter (3 × 3 gridcells) for each scan to remove high-frequency noise.

Subaerial glacier morphology

To quantify the rate of change of the glacier's subaerial terminus, we used a terrestrial radar interferometer (TRI) in August 2016

and May 2017 and time-lapse imagery in September 2018. The instruments were all deployed on a ridge to the south of the terminus throughout each field campaign (August 2016 and May 2017: 415 m above sea level, 56.8286° N, 132.3418° W; September 2018: 63 m above sea level, 56.8314° N, 132.3595° W; Fig. 1a).

Terrestrial radar interferometry

We used a Gamma Remote-Sensing TRI to measure both the glacier velocity and terminus position in August 2016 and May 2017. The TRI is a Ku band ($\lambda = 1.74$ cm) real aperture imaging radar with a maximum range of 16 km and an azimuth resolution of ~3 m in the near field (0.4 km) and ~21 m in the far field (3 km). The TRI conducted scans at ~3 min intervals over a radar swath of 120°. To enable terminus delineation, the radar backscatter images were projected into Cartesian space, georectified to UTM Zone 8N, and then gridded at 5 m (Sutherland and others, 2019). The terminus position was then manually digitized on the georectified radar backscatter images with a time separation of 2 h. To reduce location uncertainty in the terminus position, this delineation process was repeated twice. All processing of TRI data was done with Gamma proprietary software and an associated Python module (<https://bitbucket.org/luethim/gprtools>).

Time-lapse imagery

In September 2018 we used time-lapse imagery from a camera (18 mm Canon Rebel housed within a Harbortronics Time-Lapse package) with a 30 s photo interval deployed on a ridge to the south of the glacier's terminus to observe the evolution of the terminus at the waterline. The waterline position was outlined in ArcGIS for photos taken every 30 min and projected into map coordinates (UTM Zone 8N) using a camera model (Kienholz and others, 2019). The RMSE was calculated between the delineated waterline positions and closest drone-derived terminus position in time, finding uncertainty of 3 ± 2 m in the time-lapse image-derived waterlines.

Ice velocity

Glacier velocities were derived from a TRI in August 2016 and May 2017 and drone imagery in September 2018. The average ice velocity from each field campaign was extracted along the corresponding transect used for the multibeam point cloud projection and gridding (Fig. 1b; Fig. S1). To account for differences in ice velocity between the reference transect and the terminus due to strain of the ice, we additionally extract a transect of ice velocity as close to the terminus as possible and include this difference in our melt rate uncertainty estimates.

Terrestrial radar interferometry

The ice flow direction near the terminus was nearly perpendicular to the radar line-of-sight, precluding us from using interferometry to calculate near-terminus ice velocities. We instead gridded the georectified radar backscatter images at 10 m resolution and then applied normalized cross-correlation from the Python openPIV module (Bouquet, 2000) with a correlation window size of 16 × 16 pixels (160 m × 160 m) and 50% overlap to calculate ice speed (as described in Sutherland and others, 2019). The resulting velocity fields were then stacked and averaged for each field campaign.

Drone imagery

To obtain glacier velocities in September 2018, we flew 12 campaigns with a DJI Phantom IV Pro Quadcopter over the lower 130 m of the glacier. We created DEMs over the lower glacier for each campaign using Structure from Motion photogrammetric

processing in Agisoft PhotoScan (as described in Jackson and others, 2022), with ground control points on both sides of the terminus. Glacier velocity fields were generated using feature tracking in openPIV (Bouquet, 2000) of shaded relief DEMs separated by ~24 h.

Glacier change in time

To investigate the impact of environmental forcings on glacier geometry, we calculated frontal ablation (F_A) of both the subaerial terminus, using the TRI and time-lapse imagery, and the submarine terminus using the multibeam sonar data (Eqn (1)). We differenced all multibeam point clouds within a field season that had a time separation of more than 0.5 d (equivalent to 5–10 m of ice advection) to obtain the rate of change in terminus position (dL/dt). We then subtracted the terminus position change (dL/dt) from the ice velocities (U_{ice}) derived from the TRI in August 2016 and May 2017 and the drone imagery in September 2018 to give us a rate of frontal ablation (F_A), where

$$F_A(y, z, t) = U_{ice}(y, t) - \frac{dL(y, z, t)}{dt} \quad (1)$$

$$= C(y, z, t) + \dot{m}(y, z, t)$$

Frontal ablation was then separated into its two components, iceberg calving (C) and submarine melting (\dot{m}). Our calculation of submarine melt rate follows the methodology from Sutherland and others (2019), with a slightly modified approach to account for iceberg calving events that extend beneath the waterline. When calculating melt rates from multibeam sonar at LeConte Glacier in August 2016 and May 2017, Sutherland and others (2019) excluded regions of the submarine terminus where subaerial iceberg calving events were recorded with the TRI between multibeam scans. This can potentially exclude submarine melt rates from portions of the submarine terminus where subaerial calving events did not extend beneath the waterline.

Instead, here we assume that the evolution of the subaerial terminus is largely dominated by iceberg calving events in order to determine a characteristic calving rate for each field campaign by differencing successive terminus positions. Then, to remove the signal of iceberg calving from frontal ablation of the submarine terminus, we exclude gridcells where the frontal ablation rate exceeds our characteristic calving rate (10 m d⁻¹ in May 2017 and September 2018, 20 m d⁻¹ in August 2016; Fig. S2) to calculate a melt rate for each multibeam pair comparison. This has the effect of giving conservatively low estimated melt rates and allows us to evaluate melt rates across a broader range of the terminus than in Sutherland and others (2019). Using the vertical and horizontal slopes of the ice face, we converted these to an ice-perpendicular melt rate. Finally, all the multibeam pair comparisons were averaged to obtain a mean melt rate for each gridcell across the terminus for each field campaign.

Environmental forcing

Fjord water properties

We used near-terminus hydrography during each field campaign to quantify ambient ocean conditions. In August 2016 and May 2017, we collected conductivity–temperature–depth (CTD) profiles from a small vessel ~1.5 km from the glacier terminus (Sutherland and others, 2019; Jackson and others, 2022). In September 2018, our shipboard CTD observations were complemented by CTD casts collected from an autonomous kayak within 400 m of the glacier terminus (Jackson and others, 2020). To capture the ambient ocean conditions flowing towards the glacier terminus, we only look at the profiles of temperature

and salinity below the approximate depth of the thermocline in the fjord (from 75 m to the grounding line depth; Fig. S3).

Subglacial discharge

Subglacial discharge was estimated using a distributed enhanced temperature index model (Hock, 1999) coupled to an accumulation model and linear reservoir-based discharge routing model (Hock and Noetzli, 1997) as described in Amundson and others (2020). Inputs for this model include local meteorological conditions recorded with a Campbell Scientific Weather Station located near the TRI and time-lapse cameras. These data were successfully correlated with observations from the nearby (~30 km) Petersburg Airport, which allowed for the creation of a continuous time series of precipitation and temperature throughout our observation period (Sutherland and others, 2019; Fig. S4).

To identify the location across the glacier where the subglacial discharge plume would likely originate, we calculated the hydraulic pressure potential (P ; Eqn (2)) and head (H ; Eqn (3)) (Shreve, 1972):

$$P = \rho_i g(Z_I - Z_B) + \rho_w g Z_B \quad (2)$$

$$H = \frac{P}{\rho_w g} \quad (3)$$

where ρ_i and ρ_w are the densities of ice (917 kg m⁻³) and fresh water (1000 kg m⁻³), Z_I and Z_B are the elevations of the ice surface and bed relative to mean sea level and g is the acceleration due to gravity. The ice surface elevation is from a WorldView-2 DEM from 21 September 2018. The bed topography was generated using a mass-conservation approach (Morlighem and others, 2011) and validated with a seismic transect collected 7 km from the glacier's terminus (personal communication from Truffer and Motyka, 2018). Both the ice and bed data sources are gridded to the same resolution (30 m) and smoothed using a 5 × 5 cell low-pass filter to remove the influence of surface crevasses.

We then used the ArcGIS hydrology toolset to calculate the expected flow direction and upstream contribution of each grid-cell to determine the likely flow paths of subglacial streams. This output was projected into the same coordinate system as the gridded multibeam sonar data for comparison. Finally, the location of potential subglacial discharge outlets was taken to be where the highest upstream contribution values intersected with the location of the grounding line for all three field campaigns.

Results

Glacier morphology and change in time

In each field campaign, we observe terminus morphology that is distinctly 3-D and varies spatially across the subsurface terminus (see Supplementary video). In August 2016, the submarine terminus is 150 m more advanced on the northern side (Fig. 2a, line A) than on the southern side (Fig. 2a, line B). The opposite is true in May 2017 and September 2018, where the submarine terminus protrudes 70 and 90 m further into the fjord on the southern side of the terminus. In addition to these large-scale variations in terminus shape, there are smaller variations in the shape of the submarine ice face across the glacier. Although the resolution of our multibeam point clouds increases from 2016 to 2018, Figure 2a indicates that across-glacier variations in shape appear on larger spatial scales in August 2016 than in either May 2017 or September 2018. For example, in September 2018, the shape of the terminus varies on spatial scales of 100–200 m (e.g. at $x = 250$ –450 m across the terminus; Fig. 2a). In August

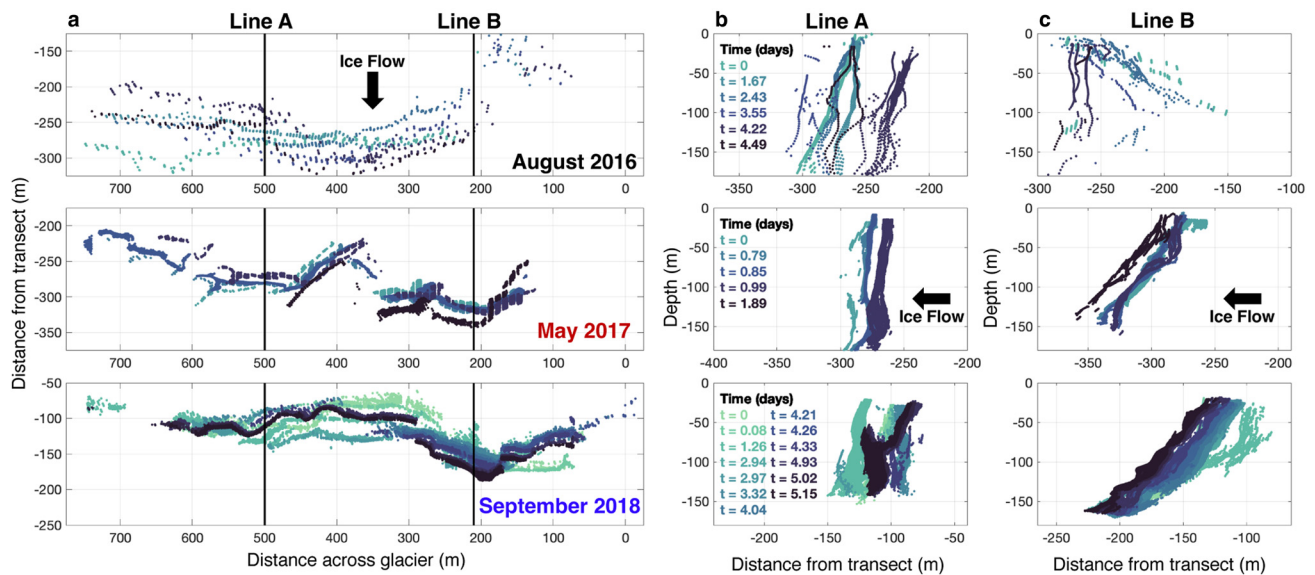


Figure 2. Short-term changes in terminus morphology for August 2016 (top), May 2017 (middle) and September 2018 (bottom). (a) Across glacier cross section taken from 100–110 m depth. Each color indicates a different multibeam scan. (b) Vertical cross section taken at 490–510 m across-glacier (line A, north side of terminus, Fig. 1b). (c) Vertical cross section taken at 200–220 m across-glacier (line B, south side of terminus, Fig. 1b). All vertical cross sections are shown in a Supplementary video.

2016, we do not see these same small-scale undulations in the terminus shape. While our multibeam point clouds can only resolve features larger than ~ 10 m, there are certainly additional smaller scale features that occur at resolutions finer than our point clouds can resolve (i.e. scallops, dimples and flutes observed on icebergs; Motyka and others, 2003; Bushuk and others, 2019).

The multibeam point clouds show that, in addition to across-glacier variations in terminus position, the terminus shape also varies with depth. In all three study periods, the shape of the terminus remains nearly vertical on the north side (line A) of the terminus (Fig. 2b). However, the terminus morphology in August 2016 is characterized by a large undercut region (100 m wide) on the south side (line B), whereas the terminus in May 2017 and September 2018 exhibits large swaths of overcut morphology (150 and 100 m wide, respectively) in the same region (Fig. 2c). These overcut regions correspond with the location of a large ice ramp that protrudes 75 m into the fjord in May 2017 and 125 m in September 2018 (Fig. 2c).

Although the general morphology of the terminus remains similar within each field campaign, the multibeam point clouds show that the submarine terminus evolves within our individual field campaigns. The multibeam point clouds show that the terminus evolves gradually over an individual study period, however, we occasionally observe instances of abrupt terminus position change, likely due to iceberg calving events that are either purely submarine or are subaerial calving events that extend beneath the waterline. An example of a subaerial calving event that includes portions of the submarine terminus can be seen on the north side of the terminus in September 2018 between the multibeam scans taken at 4.04 and 4.21 d since the start of the field campaign (Fig. 2b, bottom panel). Between these multibeam scans (taken ~ 4 h apart), the terminus retreats 30 m in the upper 75 m of the water column (light blue to dark blue line). In contrast, on the southern side of the terminus, we see the ice face slowly advance over the course of the field campaign in September 2018 (Fig. 2c, bottom panel). This pattern of advance and retreat varies across the terminus within each field campaign, with the northern side of the terminus ending in a more retreated position at the end of the field campaign and the southern side ending in a more advanced position (Fig. 2a). Despite these spatial variations,

the general morphology of the terminus (whether undercut, overcut or vertical) typically remains the same throughout an individual field campaign, with just the position of the terminus varying in time (Figs 2, 3).

In all three periods of study, the multibeam scans of the glacier terminus show slopes in the vertical direction that are majority overcut (August 2016: $52 \pm 13\%$, May 2017: $63 \pm 5\%$ and September 2018: $74 \pm 7\%$ of all gridcells on average; Fig. 3). In August 2016, the terminus became less overcut over the duration of the field campaign, with the percentage overcut changing from 70 to 49% over the 4.5 d study period (Fig. 3a). In contrast, the terminus in May 2017 and September 2018 became more overcut over the course of their individual study periods, increasing from 56 to 70% over 1.9 d (Fig. 3b) and from 67 to 73% over 5.1 d, respectively (Fig. 3c).

In addition to variations in glacier shape, the slope of the glacier terminus varies with depth and across-glacier. In all three field campaigns, the submarine terminus is close to vertical or is overcut above a depth of 70 m when averaged along the glacier front (Fig. 4a). The most significant differences in terminus morphology between each field campaign occur at depths >130 m. In August 2016, we observe undercut regions at depth, with the average slope beneath 130 m depth varying between -2° and 0° from vertical across the glacier's entire width (Fig. 4a). Below this same depth in May 2017 and September 2018, however, the submarine terminus exhibits overcut slopes varying between $6-11^\circ$ and $10-30^\circ$, respectively (Fig. 4a). The slope of the submarine terminus also varies across the width of the glacier (Fig. 4b). In August 2016, the south side of the terminus is severely undercut, with an average slope of -20° and a maximum undercut slope of -40° (Fig. 4c). The north side of the terminus, however, is overcut with an average slope of 15° . In contrast, almost all of the terminus is overcut in May 2017 and September 2018, reaching an average slope on the south side of 20° in May 2017 and September 2018.

Patterns of glacier frontal ablation (F_A) and submarine melt (m) correspond with the spatiotemporal variations in glacier morphology described above. In August 2016, maximum values of frontal ablation ($>20 \text{ m d}^{-1}$) occur directly above the deep undercut swath on the south side of the terminus (at 250–350 m

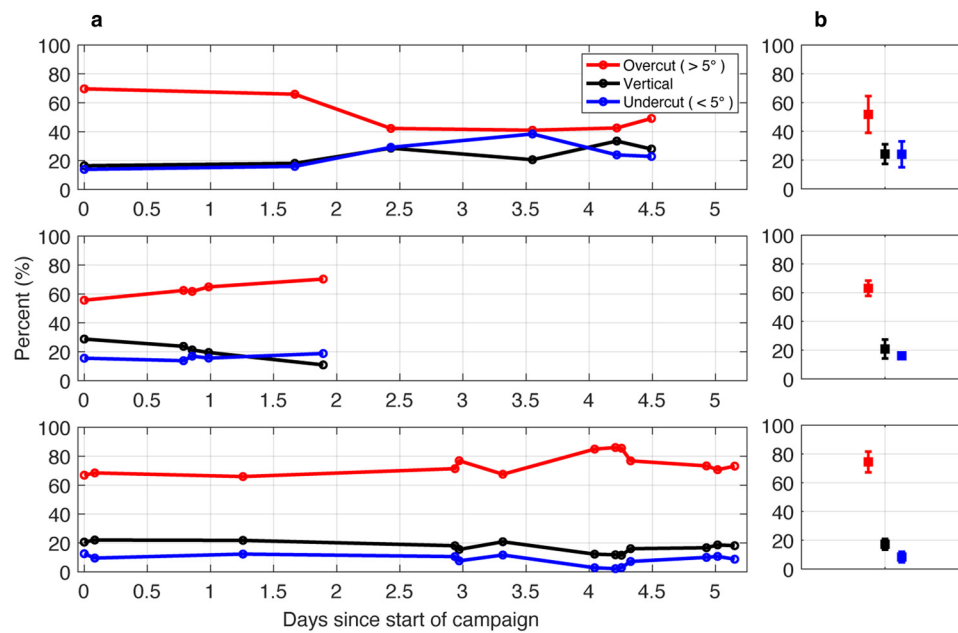


Figure 3. (a) Percentage of the terminus that is overcut (red line), vertical (black line) and undercut (blue line) over time in the field campaigns in August 2016 (top), May 2017 (middle) and September 2018 (bottom). Circle markers indicate the time at which multibeam data were collected. (b) The average percent overcut (red), vertical (black) and undercut (blue) over the duration of the field campaign with error bars indicating ± 1 std dev.

across glacier; Fig. 5a). In May 2017 and September 2018, however, frontal ablation peaks just to the north of the protruding ice ramp (at 300–400 m across glacier; Figs 5b, c). In addition to these regions of maximum frontal ablation on the south side of the terminus, the glacier experiences high localized frontal ablation in several other locations across the glacier terminus (i.e. in Fig. 5 at $x > 500$ m in August 2016, $x < 200$ m in May 2017 and $x < 150$ m and $x > 550$ m across glacier in September 2018).

After separating frontal ablation (F_A) into iceberg calving (C) and submarine melting (m), we find that the terminus in August 2016 experiences average rates of submarine melting that are $\sim 4\times$ those in May 2017 and September 2018 (August 2016: 4.84 ± 0.91 m d^{-1} ; May 2017: 1.13 ± 0.14 m d^{-1} ; September 2018: 1.85 ± 0.18 m d^{-1} ; Fig. 6). In addition, the submarine melt profile with depth shows a different spatial pattern in August 2016 than during the other two field campaigns. In all three field campaigns, the glacier

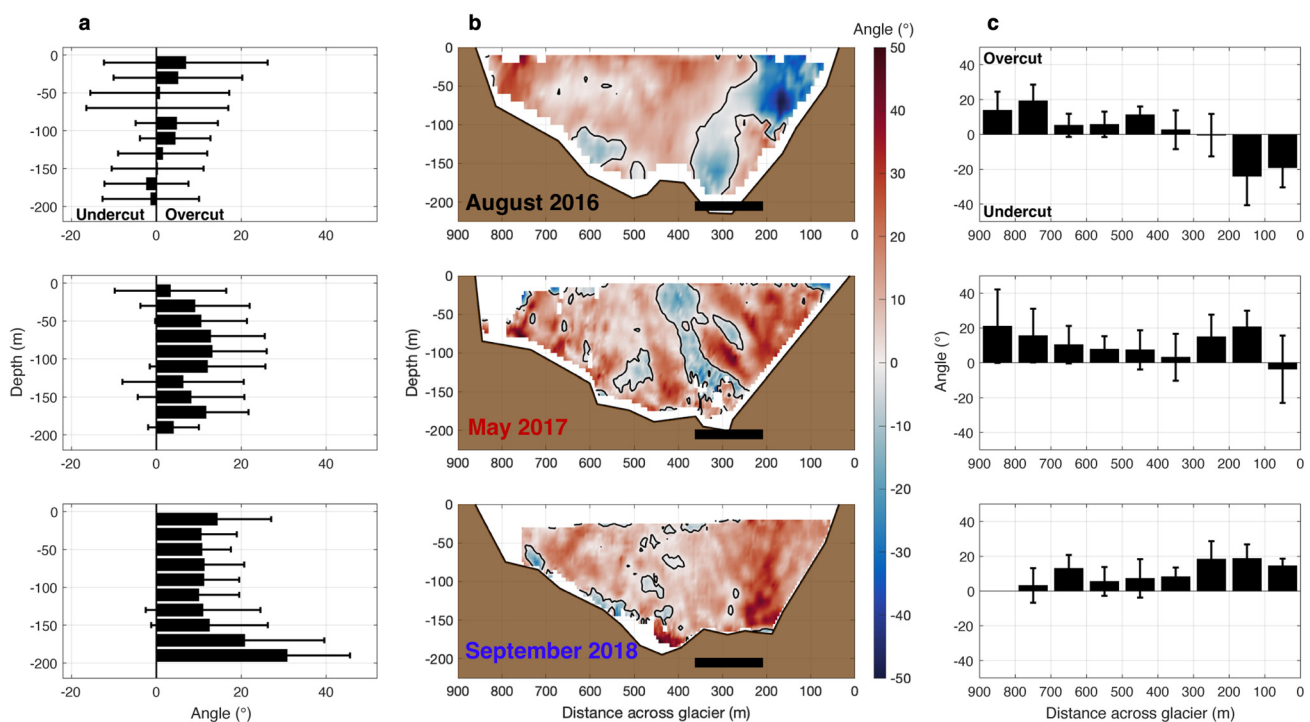


Figure 4. Average vertical terminus slope for August 2016 (top), May 2017 (middle) and September 2018 (bottom). (a) Variation in terminus slope with depth, error bars indicate ± 1 std dev. (b) Average terminus slope for each gridcell across the entire glacier terminus. (c) Variation in terminus slope across the width of the glacier. The brown shaded region indicates the bed along the grounding line of the glacier, and the black rectangle indicates the location of the likely subglacial discharge outlet, based on hydropotential analysis (Fig. 7). Angles < 0 (blue) are undercut, whereas angles > 0 (red) are overcut regions of the terminus.

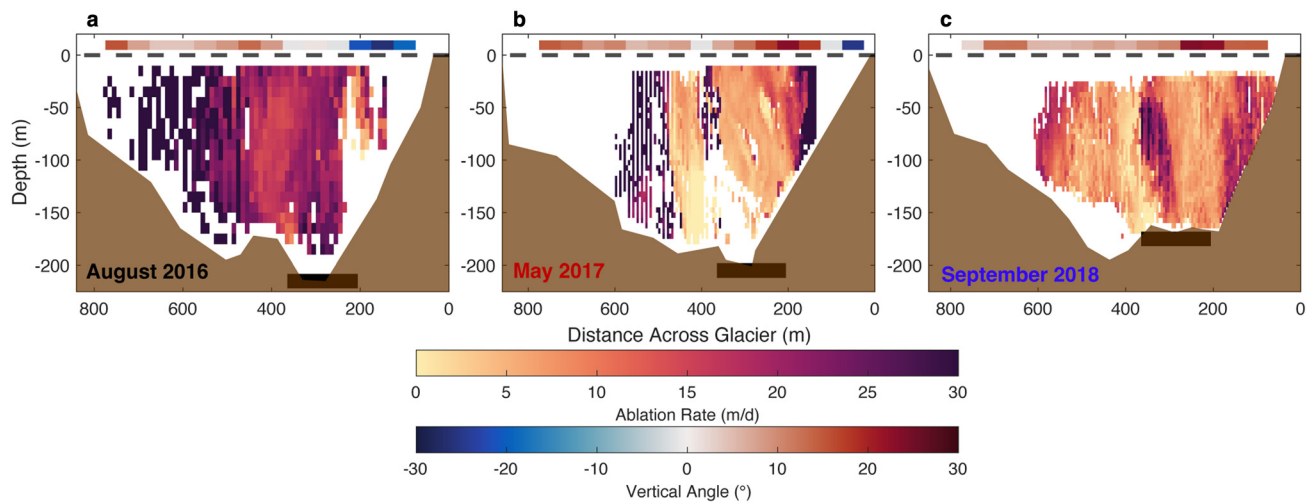


Figure 5. Plan view of average frontal ablation rates across the glacier terminus in (a) August 2016, (b) May 2017 and (c) September 2018. The brown shaded region indicates the bed along the grounding line of the glacier, and the black rectangle indicates the location of the likely subglacial discharge outlet, based on hydro-potential analysis (Fig. 7). The average vertical angle is shown in red-blue color scale above the average frontal ablation rates, where angles <0 (blue) are undercut, whereas angles >0 (red) are overcut regions of the terminus.

experiences maximum submarine melt rates at the surface of the water column, but the terminus in August 2016 experiences a secondary maximum in submarine melt rates below a depth of 130 m.

Environmental forcings

We observe significantly different environmental conditions within each individual field season (Fig. 7). The ocean temperatures below 75 m depth in the proglacial fjord are similar in August 2016 and September 2018, with an average of 7.4 ± 0.2 and $7.6 \pm 0.2^\circ\text{C}$, respectively (Fig. 7a). The ocean is considerably cooler in May 2017, with an average temperature of $3.9 \pm 0.4^\circ\text{C}$. In contrast, the average ocean salinity is highest in May 2017

($31.1 \pm 0.1 \text{ g kg}^{-1}$) and lowest in August 2016 ($26.8 \pm 0.5 \text{ g kg}^{-1}$; Fig. S3). A strong halocline is present at ~ 40 m depth in August 2016 and September 2018 but is observed at the surface in May 2017 (Fig. S3). When viewed in temperature-salinity space, these seasonal differences in temperature and salinity of the ocean show that the stratification in the fjord is most similar in August 2016 and September 2018 when compared to May 2017 (Fig. S3). These three field surveys encompass a large portion of the full yearly range of typical ocean temperatures observed within LeConte Bay as inferred from long-term mooring deployments (Hager and others, 2022).

Subglacial discharge is highest in August 2016, with a flux of $208 \pm 42 \text{ m}^3 \text{ s}^{-1}$ (Fig. 7b). May 2017 and September 2018 exhibit much lower ranges of subglacial discharge, with fluxes of 51 ± 16 and $104 \pm 33 \text{ m}^3 \text{ s}^{-1}$, respectively. These patterns align with the observed patterns in precipitation and air temperature, with the warmest and wettest conditions occurring in August 2016, and cooler temperatures occurring in both May 2017 and September 2018 (Fig. S4).

The hydropotential analysis suggests that the main subglacial discharge channel travels down the trunk of the glacier, intersecting with the southern side of the glacier's terminus at 210–360 m across glacier (indicated by 1 in Fig. 7c). In addition to this likely pathway of subglacial water, there is a second potential subglacial discharge outlet (though it is substantially less likely, with just 5% of the main channel magnitude) that is present on the northern side of the terminus at ~ 650 m across its width (indicated by 2 in Fig. 7c). By comparing to near-terminus ocean measurements from September 2018, we see that the highest ocean velocities were flowing away from the terminus between 250 and 400 m across glacier (Jackson and others, 2020), which is just north of the ice ramp protruding into the fjord.

Discussion

By conducting repeat multibeam sonar surveys of the submarine terminus at LeConte Glacier, we show that the glacier terminus is persistently overcut across three seasons and that its morphology does not change drastically within a single study period (i.e. on the timescale of a week). We find that the glacier terminus sustains large overcut geometries, such as a submarine ice ramp, in the vicinity of a subglacial discharge outlet, and discuss below the possible formation mechanisms of this terminus shape.

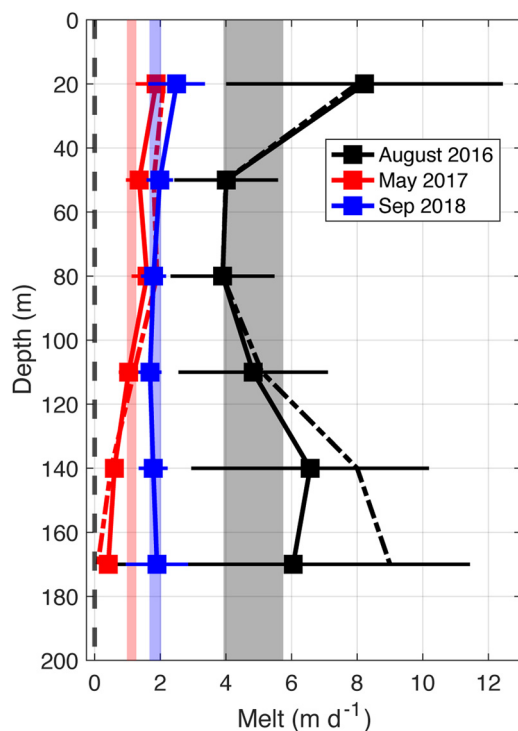


Figure 6. Average submarine melt rate with depth. Error bars indicate ± 1 std dev. Comparison to Sutherland and others (2019) is shown in dashed lines. The vertical shaded region shows the terminus area average value for each field campaign.

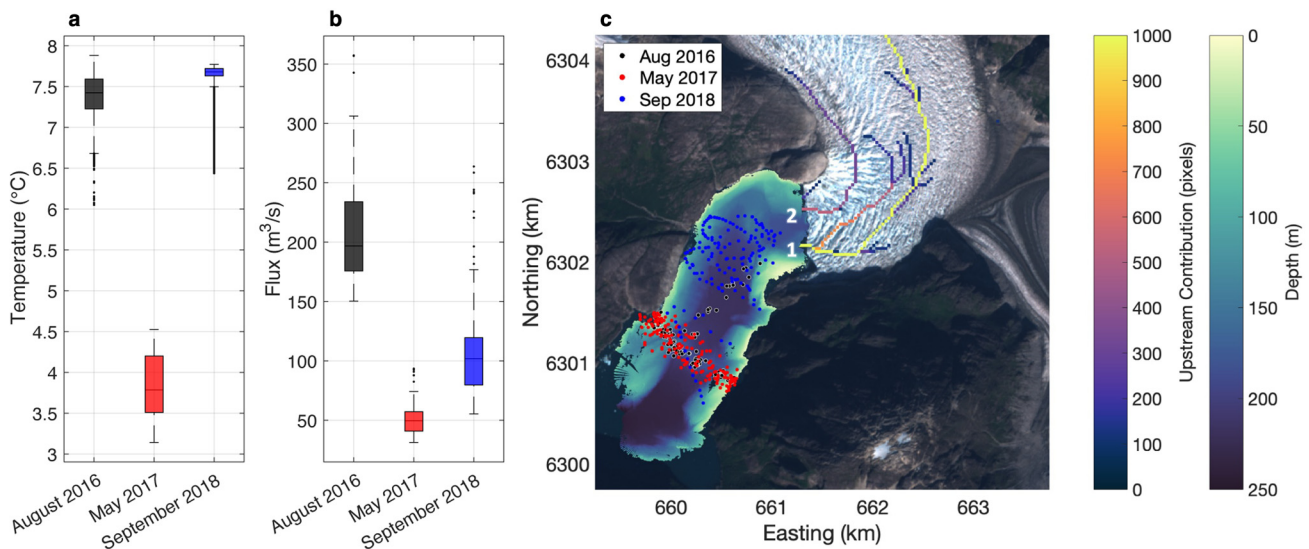


Figure 7. Overview of environmental forcings. (a) Summary of ocean temperature beneath 75 m depth for August 2016, May 2017 and September 2018. (b) Summary of subglacial discharge for 2016, 2017 and 2018. (c) Likely subglacial discharge channels as predicted by the hypopotential analysis (red-yellow color scale) and location of CTD casts taken in the proglacial fjord overlaid on top of our study area map. Channels marked by 1 and 2 indicate the discharge outlets with the highest and second highest upstream flow contribution, respectively.

Finally, we compare our multibeam-derived melt rates to previous observations at LeConte Glacier and explore the implications for plume-melt theory when a glacier terminus is overcut.

Persistent overcutting across the glacier terminus

Despite the large seasonal variations in glacier morphology and submarine melt rates observed at LeConte Glacier, the majority of the submarine terminus remains overcut through time. This is particularly notable in August 2016, when 52% of the terminus is overcut even though subglacial discharge is high ($208 \text{ m}^3 \text{ s}^{-1}$) compared to the May and September surveys (Figs 3, 7). The three field campaigns presented here encompass a wide range of the environmental conditions observed interannually at LeConte Glacier, with average subglacial discharge ranging from 51 to $208 \text{ m}^3 \text{ s}^{-1}$ (annual cycle of $\sim 20\text{--}350 \text{ m}^3 \text{ s}^{-1}$; Amundson and others, 2020) and ambient ocean temperatures between 3.9 and 7.6°C (annual cycle of $\sim 3\text{--}8^\circ\text{C}$; Hager and others, 2022). We observe a terminus morphology that is primarily overcut despite these large variations in subglacial discharge and fjord conditions.

These observations of persistent overcutting are contrary to previously published measurements of submarine glacier morphology (Rignot and others, 2015; Fried and others, 2019). Prior observations of terminus morphology come from marine-terminating outlet glaciers around the Greenland ice sheet, which typically have glacier termini that are much wider (several kilometers) and grounded deeper (100–1000 m) than LeConte Glacier (e.g. Slater and others, 2022). At these larger marine-terminating outlet glaciers, multibeam sonar-derived observations of terminus morphology revealed that the termini were largely undercut, especially in the vicinity of subglacial discharge outlets. While only 26–48% of LeConte Glacier's submarine terminus is undercut on average, undercutting was observed across 77% of the terminus at Kangerlussup Sermia (Fried and others, 2019), 76% of the terminus at Kangilernata Sermia (Rignot and others, 2015), 73% of the terminus at Store Gletscher (Rignot and others, 2015) and almost the entirety of the submarine terminus at Rink Isbræ (Rignot and others, 2015).

Due to the prevalence of undercutting previously observed at marine-terminating glaciers, models of submarine melting and iceberg calving have primarily used idealized terminus geometries that are either purely undercut or vertical (e.g. Slater and others,

2017; Holmes and others, 2023; Schulz and others, 2022). Our results, however, show that despite high melt rates observed across the glacier terminus, LeConte Glacier is largely overcut. On the northern side of the terminus, we see slight overcutting, with an average terminus slope of $\sim 12^\circ$ in all three field campaigns. The southern side of the terminus is more dramatically overcut, reaching slopes of up to $\sim 30^\circ$ from vertical (Fig. 4c). While the multibeam scans do show that the shape of the submarine terminus varies through time, the average morphology of the terminus remains nearly constant within each field campaign (with the percentage overcut varying by 13% in August 2016, 5% in May 2017 and 7% in September 2018; Fig. 3) apart from iceberg calving events that involve the submarine terminus (Fig. 2). This suggests that, on the scale of features that we can observe ($>10 \text{ m}$), the average morphology of the terminus varies much more between seasons than over shorter timescales.

Seasonal overcutting in the vicinity of a subglacial discharge outlet

Previous observations of submarine glacier termini from multibeam sonar have focused on the undercut regions adjacent to subglacial discharge outlets. However, Wagner and others (2019) observed a terminus morphology that was primarily overcut away from the influence of the subglacial discharge plume. At Saqqarliup Glacier, Greenland, the submarine portion of the terminus protruded $\sim 20 \text{ m}$ into the proglacial fjord in regions of ambient melting. This is similar to what we observe away from the subglacial discharge plume on the northern side of the terminus at LeConte Glacier (Fig. 2b). The time-varying aspect of our observations, however, show that even in the vicinity of a subglacial discharge outlet, the glacier terminus can support substantial overcut morphology through time, despite high overall melt rates (Fig. 2c).

While the majority of LeConte Glacier's terminus is overcut, there are large variations in terminus morphology between field campaigns in the vicinity of the main predicted subglacial discharge outlet. We find that periods of high subglacial discharge lead to the creation of undercut subglacial discharge outlets, and periods of lower subglacial discharge show no significant undercutting, regardless of the ocean temperature at depth

(Fig. 6). This is particularly evident on the southern side of the glacier terminus, where a 100 m undercut subglacial discharge outlet existed in August 2016 at the same location where an ice ramp protruded 125 m into the fjord during periods of low subglacial discharge in May 2017 and September 2018 (Figs 2c, 7). While the velocity field from near-glacier kayak surveying suggests that the plume rises just north of the protruding ice ramp in September 2018 (Jackson and others, 2020), we do not see evidence of an undercut subglacial discharge outlet at this location (Fig. 2b).

Although plume-melt theory would predict undercutting in the vicinity of an upwelling subglacial discharge plume due to high water velocities and ocean temperatures at the grounding line, ice ramps of similar sizes have previously been observed near subglacial discharge outlets. At Kangerlussup Sermia, multi-beam sonar revealed the presence of undercut glacier morphology near the location of subglacial discharge outlets as predicted by hydropotential gradient (Fried and others, 2015, 2019). Adjacent to one of these undercut outlets, however, was a large protrusion in the terminus of a similar aspect ratio to the ice ramp observed at LeConte Glacier (grounding line depth/overcut length ≈ 1.6).

Evidence exists for ice ramps at several marine-terminating glaciers, but these underwater protrusions have largely been ignored in models of iceberg calving and submarine melting due to the overwhelming percentage of undercutting previously observed at Greenlandic tidewater glacier termini, as well as the inability for plume-melt theory to predict submarine melt rates over an overcut ice face (as described further below). We show, however, that even during periods of high submarine melting, the submarine terminus of a tidewater glacier can be mostly overcut, and in particular, large submarine ice ramps can persist through the summer melt season.

An example of extreme overcutting: submarine ice ramps

Our observations clearly show that marine-terminating glaciers can support protruding ice ramps for substantial periods of time (Fig. 2c). Prior work has shown that ice ramps develop in models under periods of low melt (Mercenier and others, 2019, 2020), and these ice ramps have previously been observed at several grounded lake-terminating glaciers in New Zealand (Dykes and others, 2011; Robertson and others, 2012; Purdie and others, 2016) and Patagonia (Warren and others, 2001; Sugiyama and others, 2019), as well as at grounded marine-terminating glaciers in Alaska (Hunter and Powell, 1998) and Greenland (Chauché and others, 2014; Rignot and others, 2015). The occurrence of large submarine calving events previously at LeConte Glacier (Motyka, 1997; Motyka and others, 1998) suggests that these ice ramps could extend 200–300 m into the proglacial fjord and be a regular occurrence at this tidewater glacier, despite the high melt rates.

While investigating the formation of these ice ramps is beyond the scope of this study, several lines of observational evidence suggest potential mechanisms for their formation and persistence. The depth-varying profile of submarine melting at LeConte Glacier presented here, and in Sutherland and others (2019), shows elevated submarine melt rates at the surface in May 2017 and September 2018 (Fig. 6). If you start with a vertical terminus, a difference in melt rate between the surface and grounding line of 1.5 m d^{-1} could form an ice ramp of the size observed (150 m) in 100 d purely from submarine melting. With the addition of sub-aerial calving events that extend beneath the waterline and sediment insulating the ice near the grounding line (e.g. Hunter and Powell, 1998), this ice ramp could form even quicker. Between May 2017 and September 2018, Eidam and others

(2020) observed the formation of a sediment mound $\sim 40 \text{ m}$ thick that advanced with the glacier at the location of the protruding ice ramp. It is possible that the ice ramp extended beneath the surface of this sediment mound, making it larger than appears in our multibeam point clouds of the ice face. This additional sediment could have insulated the lower portion of the ice ramp and counteracted buoyancy forces, allowing it to persist, and even grow, despite having just gone through a summer melt season.

In addition to insulation from sediment, melt rates are likely enhanced towards the surface of the water column by a more energetic velocity field in the upper ocean, as suggested by near-terminus ocean observations at LeConte Glacier. In addition to horizontal recirculations, or eddies, driven by the outflowing discharge plume (Slater and others, 2018; Kienholz and others, 2019), near-glacier moorings have revealed the presence of internal waves, excited by the upwelling subglacial discharge plume, that enhance velocities across the terminus (Cusack and others, *in press*). Both the near-glacier moorings (Cusack and others, *in press*) and surveying with kayaks (Fig. S7 in Jackson and others, 2020) show that the kinetic energy of the along-ice flow increases towards the surface, which should lead to elevated submarine melt rates towards the surface and contribute to the formation of an ice ramp over time. Near surface enhancement of subaqueous melt has also been suggested at lake-terminating glaciers, whereby atmospherically warmed surface waters cause enhanced melt rates at the top of the water column, resulting in the formation of ice terraces (Sugiyama and others, 2019). However, ice terraces are typically characterized by abrupt changes in slope beneath the surface warmed layer, in direct contrast with the gradual overcut slope observed at the ice ramp at LeConte Glacier (Fig. 2c).

These ice ramps are not currently represented in models of near-terminus glacier dynamics and change (e.g. Brinkerhoff and others, 2017; Cowton and others, 2019; Ma and Bassis, 2019; Slater and others, 2021). In addition, modeling of the ice–ocean interface typically only includes terminus morphologies that are either purely vertical or are undercut (e.g. Slater and others, 2017, 2021). Together, this suggests that we are missing an important process in understanding the evolution of glacier termini. Recent modeling investigations into near-terminus glacier dynamics have found that, depending on the profile of submarine melting and the resulting terminus morphology, iceberg calving fluxes can either be enhanced (resulting in a ‘calving multiplier’) or suppressed due to non-linear relationships between the morphology and ice flow (O’Leary and Christoffersen, 2013; Wagner and others, 2016; Ma and Bassis, 2019). Therefore, having realistic constraints on the shape of glacier termini beneath the waterline to input into these models is essential for understanding the glacier evolution through time.

Further evidence for elevated submarine melt rates

While our results are only the second instance of direct melt rate estimates from repeat multibeam sonar imaging, the elevated melt rates described in this study are in line with other recently published estimates from LeConte Glacier (Sutherland and others, 2019; Jackson and others, 2020, 2022). Sutherland and others (2019) calculated submarine melt rates for all portions of the terminus where the glacier did not calve subaerially between scans in August 2016 and May 2017. Our thresholding method allowed us to estimate melt rates for portions of the terminus that experienced subaerial iceberg calving that did not extend beneath the waterline. Despite these different methodologies, the melt rates described here closely match those described in Sutherland and others (2019; Fig. 6). In September 2018, our estimated melt rates are $1\text{--}2 \text{ m d}^{-1}$ lower than those determined by near-

terminus hydrographic observations (Jackson and others, 2020). For all three field campaigns, the meltwater volume flux derived from the flux-gate method results in submarine melt rates of 5–18 m d⁻¹ (Jackson and others, 2022). While the submarine melt rates derived from ocean observations are larger than those estimated from multibeam sonar, Jackson and others (2022) note that the multibeam-derived melt rates are likely biased low due to incomplete coverage of the terminus, particularly in the vicinity of the upwelling of the subglacial discharge plume, where turbid, fast-flowing water makes acoustic mapping difficult. In addition, the flux-gate method is likely biased high if melt from icebergs contributes to the meltwater flux between the ocean transect and glacier terminus. Regardless, the vast discrepancy between the submarine melt rates derived from observations at LeConte Glacier and those derived by plume-melt theory suggests that modifications to standard parameterizations are needed (Jackson and others, 2022).

In addition to the magnitude of submarine melt, our observations support other recent results from LeConte Glacier showing that submarine melt is much more sensitive to the amount of subglacial discharge and resulting near-glacier ocean currents than it is to ocean temperature (Jackson and others, 2020, 2022). In August 2016 the glacier experienced average submarine melt rates that were 2.6 times higher than those in September 2018, despite similar ocean temperatures at the time of data collection (Figs 6, 7a). Instead, the glacier in September 2018 had comparable melt rates to May 2017, when the ocean temperature was two times lower (Figs 6, 7a), suggesting that ocean thermal forcing is not the main control on the rate of ice melt. Instead, the flux of subglacial discharge in August 2016 was two times higher than that in September 2018 and four times higher than that in May 2017 (Fig. 7b), supporting the recent findings that subglacial discharge plays a much larger role than ambient ocean temperature in controlling the submarine melt rates of glacier termini.

Our results suggest two potential reasons for the discrepancy between plume-melt theory and observed melt rates: secondary circulation in the fjord and the persistent overcutting of the submarine terminus. The influence of subglacial discharge may currently be underestimated by plume-melt theory because the upwelling of plumes not only influences the vertical velocity of the water column but can also induce secondary circulation in the fjord due to internal waves (Cusack and others, *in press*) and horizontal circulation (Slater and others, 2018; Kienholz and others, 2019). By including horizontal water velocities in plume-melt theory at LeConte Glacier, Jackson and others (2020) found that melt rates were two orders of magnitude greater than standard theory predicts and more closely matched observations. This could explain why even away from the upwelling discharge plume, we observe elevated submarine melt rates (described above; Sutherland and others, 2019). Furthermore, the discrepancy between theory and observations could be affected by the overcutting of the glacier itself, as discussed below.

Implications of overcut terminus morphology on plume-melt theory

Our observations of seasonal variations in terminus morphology and submarine frontal ablation suggest that feedbacks between glacier shape and its rate of change might exist. The highest frontal ablation rates in August 2016 occur directly above the location of the subglacial discharge outlet on the southern side of the terminus (Fig. 5a), suggesting the plume upwells along the undercut ice face. During periods of low subglacial discharge, however, frontal ablation rates reach a maximum on either side of the protruding ice ramp (Figs 5b, c). Near-terminus ocean measurements (Jackson and others, 2020) support our observations

that the upwelling discharge plume was shifted to the north of the ice ramp, suggesting that the shape of the submarine terminus can alter the path of the glacial plume as it upwells along the face of the glacier and cause spatial variations in the submarine melt rate.

The interaction between upwelling plumes, the ice–ocean boundary layer and overcut terminus morphology are currently unexplored. Previous work examining plume and boundary layer dynamics has been exclusively focused on the parameter space from no slope (i.e. beneath sea ice or an ice shelf; Jenkins, 1991) to vertical slope (i.e. idealized tidewater glacier termini; Kerr and McConnochie, 2015). Within this parameter space of zero to vertical slope, studies have found that the slope can affect the entrainment in subglacial discharge plumes and associated melt rates (Jenkins, 2011; Slater and others, 2017). In addition, the slope of the ice–ocean boundary layer has been shown to influence the distance over which the transition from laminar to turbulent flow occurs (Malyarenko and others, 2020). However, it is currently unknown how overcut terminus morphologies interact with the ice–ocean boundary layer and upwelling plumes.

An overcut terminus might pose several challenges to the theoretical underpinnings of plume-melt theory. First, plume-melt theory couples buoyant plume theory with the three-equation melt parameterization, under the assumption that the plume stays attached to the wall (due to the Coanda effect) and thus plume velocities control boundary layer transports (Jenkins, 1991, 2011). If the terminus slope is moderately overcut, it is possible that the Coanda effect would continue to take place, drawing the upwelling plume towards the ice face (Kimura and others, 2014). However, if the ice face is sufficiently overcut, buoyant plumes could detach from the glacier terminus as they upwell, uncoupling the plume from the boundary layer. Second, the three-equation melt parameterization assumes that shear instabilities – as opposed to convective instabilities – control fluxes of heat and salt across the inner boundary layer (Holland and Jenkins, 1999; Malyarenko and others, 2020). While the validity of this assumption has been explored for vertical ice fronts (e.g. McConnochie and Kerr, 2017), it might be even more problematic at overcut ice. Thus, both the boundary layer dynamics and the representation of the outer velocity field could be significantly misrepresented if standard plume-melt theory is applied to overcut ice.

The detachment of plumes from the ice front would not only affect the melt rates but also the evolution of the plumes themselves. In this regime, the upwelling melt plume would act more like a classical buoyant plume rising with entrainment on all sides. Unbounded by a glacier face, the rising plume would have approximately twice the surface area and entrainment (e.g. Ezhova and others, 2018), increasing its volume flux and reaching its depth of neutral buoyancy more rapidly.

We speculate that overcutting, with plumes detaching from the ice face, might lead to more efficient export of meltwater from the boundary layer. This would weaken the insulating buffer of cold, fresh water that accumulates near the ice–ocean interface, potentially enhancing heat and salt transfer across the boundary layer and elevating rates of submarine melt. More detailed observations of the ice–ocean boundary layer and near-terminus ocean currents are needed to better understand how the overcutting of glacier termini might affect the boundary layer dynamics and evolution of the upwelling plumes.

Conclusions

Reconciling the drivers of ocean-induced glacier change has remained elusive due to the difficulty of observing terminus geometry beneath the waterline. This work provides the first observations of time-varying terminus morphology and uses

concurrent measurements of environmental forcings to show that, despite high subglacial discharge and ocean temperatures, the majority of the terminus at LeConte Glacier is overcut. In addition, we show that the location of and flux from subglacial discharge outlets acts as a key control on submarine terminus change, with the southern side of the terminus sustaining a large ice ramp in periods of low discharge, despite its proximity to the discharge outlet. Our results show that submarine melt rates were relatively high in summer (August 2016) when subglacial discharge was at a maximum, and lowest in late spring (May 2017) when the discharge was low, in line with theoretical predictions that submarine melt rates highly depend on the magnitude of subglacial discharge emerging at the grounding line.

While our results support the dependence of submarine melt on subglacial discharge, the submarine melt rates we find confirm recent ocean and acoustic observations that suggest overall submarine melt rates are up to two orders of magnitude higher than standard plume-melt theory predicts at LeConte Glacier. The persistent overcutting of LeConte Glacier's submarine terminus provides challenges for current implementations of plume-melt theory to estimate submarine melt rates, as the understanding of buoyant plume and ice–ocean boundary layer dynamics in a regime of overcut ice slopes is largely unexplored.

The dynamic nature of the submarine terminus has implications for the path of near-terminus ocean currents, glacier stresses and potentially calving dynamics. Our findings challenge the assumption that the terminus is either purely vertical or undercut across its width. More long-term observations of submarine terminus morphology, grounding line bathymetry and near-terminus ocean conditions are necessary to obtain a process-based understanding of the mechanisms that control the evolution of the submarine terminus and the timescales of these changes. In the future, combining this with measurements of the subaerial terminus will allow further investigation of the feedbacks between submarine melting and glacier morphology, resulting in a better understanding of the influence that submarine glacier change plays in near-terminus glacier dynamics.

Supplementary material. The supplementary material for this article can be found at <https://doi.org/10.1017/aog.2023.38>.

Acknowledgements. Funding was provided by National Science Foundation grants OPP-1503910, 1504191, 1504288, 2023269 and 2023319. We thank the captain and the crew of the *MV Stellar* and Scott Hursey for their contribution to the field data collection. The authors thank Petersburg High School and the U.S. Forest Service for accommodating this project. We thank Alex Hager, Eric Skillingstad, Meagan Wengrove, Jesse Cusack and Nadia Cohen for useful discussions on the relationship between glacier morphology and submarine melt. Valuable feedback from Adrian Jenkins, Shin Sugiyama, Till Wagner and one anonymous reviewer significantly improved the quality and clarity of this manuscript. The authors also acknowledge the Shatx'héen Kwáan Tlingits, whose ancestral lands lie in this region. All data presented in this manuscript are available from the author upon request.

References

- Amaral T, Bartholomaeus TC and Enderlin EM** (2020) Evaluation of iceberg calving models against observations from Greenland outlet glaciers. *Journal of Geophysical Research: Earth Surface* **125**, 1–29. doi: [10.1029/2019JF005444](https://doi.org/10.1029/2019JF005444).
- Amundson JM and 6 others** (2020) Formation, flow and break-up of ephemeral ice mélange at LeConte Glacier and Bay, Alaska. *Journal of Glaciology*, 1–14. doi: [10.1017/jog.2020.29](https://doi.org/10.1017/jog.2020.29).
- Benn DI and 7 others** (2017) Melt-under-cutting and buoyancy-driven calving from tidewater glaciers: new insights from discrete element and continuum model simulations. *Journal of Glaciology* **63**(240), 691–702. doi: [10.1017/jog.2017.41](https://doi.org/10.1017/jog.2017.41).
- Benn DI, Warren CR and Mottram RH** (2007) Calving processes and the dynamics of calving glaciers. *Earth-Science Reviews* **82**, 143–179. doi: [10.1016/j.earscirev.2007.02.002](https://doi.org/10.1016/j.earscirev.2007.02.002).
- Bouquet J-Y** (2000) Pyramidal implementation of the Affine Lucas Kanade Feature Tracker description of the algorithm. Open CV Document, Intel, Microprocessor Research Labs.
- Brinkerhoff D, Truffer M and Aschwanden A** (2017) Sediment transport drives tidewater glacier periodicity. *Nature Communications* **8**, 90. doi: [10.1038/s41467-017-00095-5](https://doi.org/10.1038/s41467-017-00095-5).
- Bushuk M, Holland DM, Stanton TP, Stern A and Gray C** (2019) Ice scallops: a laboratory investigation of the ice–water interface. *Journal of Fluid Mechanics* **873**(2), 942–976. doi: [10.1017/jfm.2019.398](https://doi.org/10.1017/jfm.2019.398).
- Carroll D and 11 others** (2016) The impact of glacier geometry on meltwater plume structure and submarine melt in Greenland fjords. *Geophysical Research Letters* **43**, 9739–9748. doi: [10.1002/2016GL070170](https://doi.org/10.1002/2016GL070170).
- Catania GA and 7 others** (2018) Geometric controls on tidewater glacier retreat in central western Greenland. *Journal of Geophysical Research: Earth Surface* **123**(8), 2024–2038. doi: [10.1029/2017JF004499](https://doi.org/10.1029/2017JF004499).
- Chauché N and 8 others** (2014) Ice–ocean interaction and calving front morphology at two west Greenland tidewater outlet glaciers. *The Cryosphere* **8**(4), 1457–1468. doi: [10.5194/tc-8-1457-2014](https://doi.org/10.5194/tc-8-1457-2014).
- Cowton T, Slater D, Sole A, Goldberg D and Nienow P** (2015) Modeling the impact of glacial runoff on fjord circulation and submarine melt rate using a new subgrid-scale parameterization for glacial plumes. *Journal of Geophysical Research: Oceans* **120**(2), 796–812. doi: [10.1002/2014JC010324](https://doi.org/10.1002/2014JC010324).
- Cowton TR, Todd JA and Benn DI** (2019) Sensitivity of tidewater glaciers to submarine melting governed by plume locations. *Geophysical Research Letters* **46**, 11219–11227. doi: [10.1029/2019GL084215](https://doi.org/10.1029/2019GL084215).
- Cusack JM and 7 others** (in press) Internal waves excited by subglacial discharge: implications for tidewater glacier melt. *Geophysical Research Letters*. doi: [10.1029/2022GL102426](https://doi.org/10.1029/2022GL102426).
- Dykes R, Brook M, Robertson C and Fuller I** (2011) Twenty-first century calving retreat of Tasman Glacier, Southern Alps, New Zealand. *Arctic, Antarctic, and Alpine Research* **43**(1), 1–10. doi: [10.1657/1938-4246-43.1.1](https://doi.org/10.1657/1938-4246-43.1.1).
- Eidam EF and 5 others** (2020) Moraine bank evolution and impact on terminus dynamics during a tidewater glacier stillstand. *Journal of Geophysical Research: Earth Surface* **125**(11), 1–20. doi: [10.1029/2019JF005359](https://doi.org/10.1029/2019JF005359).
- Enderlin EM and 5 others** (2014) An improved mass budget for the Greenland ice sheet. *Geophysical Research Letters* **41**, 866–872. doi: [10.1002/2013GL059010](https://doi.org/10.1002/2013GL059010).
- Ezhova E, Cenedese C and Brandt L** (2018) Dynamics of three-dimensional turbulent wall plumes and implications for estimates of submarine glacier melting. *Journal of Physical Oceanography* **48**(9), 1941–1950. doi: [10.1175/JPO-D-17-0194.1](https://doi.org/10.1175/JPO-D-17-0194.1).
- Fried MJ and 6 others** (2019) Distinct frontal ablation processes drive heterogeneous submarine terminus morphology. *Geophysical Research Letters* **46**(21), 12083–12091. doi: [10.1029/2019GL083980](https://doi.org/10.1029/2019GL083980).
- Fried MJ and 8 others** (2015) Distributed subglacial discharge drives significant submarine melt at a Greenland tidewater glacier. *Geophysical Research Letters* **42**(21), 9328–9336. doi: [10.1002/2015GL065806](https://doi.org/10.1002/2015GL065806).
- Hager AO and 6 others** (2022) Subglacial discharge reflux and buoyancy forcing drive seasonality in a silled glacial fjord. *Journal of Geophysical Research: Oceans* **127**(5), 1–21. doi: [10.1029/2021JC018355](https://doi.org/10.1029/2021JC018355).
- Hock R** (1999) A distributed temperature-index ice- and snowmelt model including potential direct solar radiation. *Journal of Glaciology* **45**(149), 101–111.
- Hock R and Noetzi C** (1997) Areal melt and discharge modelling of Storgläciären, Sweden. *Annals of Glaciology* **24**, 211–216.
- Holland DM and Jenkins A** (1999) Modeling thermodynamic ice–ocean interactions at the base of an ice shelf. *Journal of Physical Oceanography* **29**(8), 1787–1800.
- Holland DM, Thomas RH, De Young B, Ribergaard MH and Lyberth B** (2008) Acceleration of Jakobshavn Isbræ triggered by warm subsurface ocean waters. *Nature Geoscience* **1**, 659–664. doi: [10.1038/ngeo316](https://doi.org/10.1038/ngeo316).
- Holmes FA, van Dongen E, Noormets R, Pelticki M and Kirchner N** (2023) Impact of tides on calving patterns at Kronebreen, Svalbard – insights from three-dimensional ice dynamical modelling. *The Cryosphere* **17**, 1853–1872. <https://doi.org/10.5194/tc-17-1853-2023>.
- How P and 8 others** (2019) Calving controlled by melt-under-cutting: detailed calving styles revealed through time-lapse observations. *Annals of Glaciology* **60**(78), 20–31. doi: [10.1017/aog.2018.28](https://doi.org/10.1017/aog.2018.28).
- Howat IM, Joughin I, Fahnestock M, Smith BE and Scambos TA** (2008) Synchronous retreat and acceleration of southeast Greenland outlet glaciers 2000–06: ice dynamics and coupling to climate. *Journal of Glaciology* **54**(187), 646–660. doi: [10.3189/002214308786570908](https://doi.org/10.3189/002214308786570908).

- Hunter LE and Powell RD (1998) Ice foot development at temperate tidewater margins in Alaska. *Geophysical Research Letters* **25**(11), 1923–1926. doi: [10.1029/98GL01403](https://doi.org/10.1029/98GL01403).
- Jackson RH and 6 others (2022) The relationship between submarine melt and subglacial discharge from observations at a tidewater glacier. *Journal of Geophysical Research: Oceans* **127**(10), 1–22. doi: [10.1029/2021JC018204](https://doi.org/10.1029/2021JC018204).
- Jackson RH and 8 others (2020) Meltwater intrusions reveal mechanisms for rapid submarine melt at a tidewater glacier. *Geophysical Research Letters* **47**. doi: [10.1029/2019GL085335](https://doi.org/10.1029/2019GL085335).
- Jenkins A (1991) A one-dimensional model of ice shelf–ocean interactions. *Journal of Geophysical Research* **96**(C11), 20,671–20,677.
- Jenkins A (1999) The impact of melting ice on ocean waters. *Journal of Physical Oceanography* **29**, 2370–2381.
- Jenkins A (2011) Convection-driven melting near the grounding lines of ice shelves and tidewater glaciers. *Journal of Physical Oceanography* **41**(12), 2279–2294. doi: [10.1175/JPO-D-11-03.1](https://doi.org/10.1175/JPO-D-11-03.1).
- Kerr RC and McConnochie CD (2015) Dissolution of a vertical solid surface by turbulent compositional convection. *Journal of Fluid Mechanics* **765**, 211–228. doi: [10.1017/jfm.2014.722](https://doi.org/10.1017/jfm.2014.722).
- Kienholz C and 9 others (2019) Tracking icebergs with time-lapse photography and sparse optical flow, LeConte Bay, Alaska, 2016–2017. *Journal of Glaciology* **65**(250), 195–211. doi: [10.1017/jog.2018.105](https://doi.org/10.1017/jog.2018.105).
- Kimura S, Holland PR, Jenkins A and Piggott M (2014) The effect of meltwater plumes on the melting of a vertical glacier face. *Journal of Physical Oceanography* **44**(12), 3099–3117. doi: [10.1175/JPO-D-13-0219.1](https://doi.org/10.1175/JPO-D-13-0219.1).
- Kochitzky W and 17 others (2022) The unquantified mass loss of Northern Hemisphere marine-terminating glaciers from 2000–2020. *Nature Communications* **13**(1), 5835. doi: [10.1038/s41467-022-33231-x](https://doi.org/10.1038/s41467-022-33231-x).
- Ma Y and Bassis JN (2019) The effect of submarine melting on calving from marine terminating glaciers. *Journal of Geophysical Research: Earth Surface* **124**, 334–346. doi: [10.1029/2018JF004820](https://doi.org/10.1029/2018JF004820).
- Malyarenko A and 5 others (2020) A synthesis of thermodynamic ablation at ice–ocean interfaces from theory, observations and models. *Ocean Modelling* **154**, 101692. doi: [10.1016/j.ocemod.2020.101692](https://doi.org/10.1016/j.ocemod.2020.101692).
- McConnochie CD and Kerr RC (2017) Testing a common ice–ocean parameterization with laboratory experiments. *Journal of Geophysical Research: Oceans* **122**(7), 5905–5915. doi: [10.1002/2017JC012918](https://doi.org/10.1002/2017JC012918).
- Mercenier R, Lüthi MP and Vieli A (2019) A transient coupled ice flow–damage model to simulate iceberg calving from tidewater outlet glaciers. *Journal of Advances in Modeling Earth Systems* **11**(9), 3057–3072. doi: [10.1029/2018MS001567](https://doi.org/10.1029/2018MS001567).
- Mercenier R, Lüthi MP and Vieli A (2020) How oceanic melt controls tidewater glacier evolution. *Geophysical Research Letters* **47**. doi: [10.1029/2019GL086769](https://doi.org/10.1029/2019GL086769).
- Morlighem M and 5 others (2011) A mass conservation approach for mapping glacier ice thickness. *Geophysical Research Letters* **38**(19), 1–6. doi: [10.1029/2011GL048659](https://doi.org/10.1029/2011GL048659).
- Motyka R (1997) *Deep-Water Calving at Le Conte Glacier, Southeast Alaska*. Ohio: Byrd Polar Research Center, The Ohio State University, Columbus.
- Motyka RJ, Begét J and Bowen P (1998) Recent retreat of LeConte Glacier and associated calving and iceberg hazards. Alaska Division of Geological & Geophysical Surveys Report of Investigation, 98-15, 9 p. doi: [10.14509/2590](https://doi.org/10.14509/2590).
- Motyka RJ, Dryer WP, Amundson J, Truffer M and Fahnestock M (2013) Rapid submarine melting driven by subglacial discharge, LeConte Glacier, Alaska. *Geophysical Research Letters* **40**, 5153–5158. doi: [10.1002/grl.51011](https://doi.org/10.1002/grl.51011).
- Motyka R, Hunter L, Echelmeyer KA and Connor C (2003) Submarine melting at the terminus of a temperate tidewater glacier, LeConte Glacier, Alaska, U.S.A. *Annals of Glaciology* **36**, 57–65.
- Mouginot J and 8 others (2019) Forty-six years of Greenland ice sheet mass balance from 1972 to 2018. *Proceedings of the National Academy of Sciences of the United States of America* **116**(19), 9239–9244. doi: [10.1073/pnas.1904242116](https://doi.org/10.1073/pnas.1904242116).
- O’Leary M and Christoffersen P (2013) Calving on tidewater glaciers amplified by submarine frontal melting. *The Cryosphere* **7**, 119–128. doi: [10.5194/tc-7-119-2013](https://doi.org/10.5194/tc-7-119-2013).
- O’Neal S, Echelmeyer KA and Motyka RJ (2001) Short-term flow dynamics of a retreating tidewater glacier: LeConte Glacier, Alaska, U.S.A. *Journal of Glaciology* **47**(159), 567–578. doi: [10.3189/172756501781831855](https://doi.org/10.3189/172756501781831855).
- Podrasky D, Truffer M, Lüthi M and Fahnestock M (2014) Quantifying velocity response to ocean tides and calving near the terminus of Jakobshavn Isbræ, Greenland. *Journal of Glaciology* **60**(222), 609–621. doi: [10.3189/2014JG13J130](https://doi.org/10.3189/2014JG13J130).
- Purdie H, Bealing P, Tidey E, Gomez C and Harrison J (2016) Bathymetric evolution of Tasman Glacier terminal lake, New Zealand, as determined by remote surveying techniques. *Global and Planetary Change* **147**, 1–11. doi: [10.1016/j.gloplacha.2016.10.010](https://doi.org/10.1016/j.gloplacha.2016.10.010).
- Rignot E, Fenty I, Xu Y, Cai C and Kemp C (2015) Undercutting of marine-terminating glaciers in west Greenland. *Geophysical Research Letters* **42**, 5909–5917. doi: [10.1002/2015GL064236](https://doi.org/10.1002/2015GL064236).
- Robertson CM, Benn DI, Brook MS, Fuller IC and Holt KA (2012) Subaqueous calving margin morphology at Mueller, Hooker and Tasman glaciers in Aoraki/Mount Cook National Park, New Zealand. *Journal of Glaciology* **58**(212), 1037–1046. doi: [10.3189/2012JG12J048](https://doi.org/10.3189/2012JG12J048).
- Schulz K, Nguyen AT and Pillar HR (2022) An improved and observationally-constrained melt rate parameterization for vertical ice fronts of marine terminating glaciers. *Geophysical Research Letters* **49**. doi: [10.1029/2022gl100654](https://doi.org/10.1029/2022gl100654).
- Shreve RL (1972) Movement of water in glaciers. *Journal of Glaciology* **11**(62), 205–214. doi: [10.3189/s002214300002219x](https://doi.org/10.3189/s002214300002219x).
- Slater DA and 5 others (2018) Localized plumes drive front-wide ocean melting of a Greenlandic tidewater glacier. *Geophysical Research Letters* **45**, 12,350–12,358. doi: [10.1029/2018GL080763](https://doi.org/10.1029/2018GL080763).
- Slater DA, Benn DI, Cowton TR, Bassis JN and Todd JA (2021) Calving multiplier effect controlled by melt undercut geometry. *Journal of Geophysical Research: Earth Surface* **126**(7), 1–17. doi: [10.1029/2021JF006191](https://doi.org/10.1029/2021JF006191).
- Slater DA and 7 others (2022) Characteristic depths, fluxes, and timescales for Greenland’s tidewater glacier fjords from subglacial discharge-driven upwelling during summer. *Geophysical Research Letters* **49**(10), 1–9. doi: [10.1029/2021GL097081](https://doi.org/10.1029/2021GL097081).
- Slater DA, Nienow PW, Cowton TR, Goldberg DN and Sole AJ (2015) Effect of near-terminus subglacial hydrology on tidewater glacier submarine melt rates. *Geophysical Research Letters* **42**, 2861–2868. doi: [10.1080/10550887.2011.581988](https://doi.org/10.1080/10550887.2011.581988).
- Slater DA, Nienow PW, Goldberg DN, Cowton TR and Sole AJ (2017) A model for tidewater glacier undercutting by submarine melting. *Geophysical Research Letters* **44**, 2360–2368. doi: [10.1002/2016GL072374](https://doi.org/10.1002/2016GL072374).
- Straneo F and 15 others (2013) Challenges to understanding the dynamic response of Greenland’s marine terminating glaciers to oceanic and atmospheric forcing. *Bulletin of the American Meteorological Society* **94**(8), 1131–1144. doi: [10.1175/BAMS-D-12-00100.1](https://doi.org/10.1175/BAMS-D-12-00100.1).
- Sugiyama S, Minowa M and Schaefer M (2019) Underwater ice terrace observed at the front of Glacier Grey, a freshwater calving glacier in Patagonia. *Geophysical Research Letters* **46**(5), 2602–2609. doi: [10.1029/2018GL081441](https://doi.org/10.1029/2018GL081441).
- Sutherland DA and 8 others (2019) Direct observations of submarine melt and subsurface geometry at a tidewater glacier. *Science* **365**, 369–374. doi: [10.1126/science.aax3528](https://doi.org/10.1126/science.aax3528).
- Van Den Broeke MR and 7 others (2016) On the recent contribution of the Greenland ice sheet to sea level change. *The Cryosphere* **10**, 1933–1946. doi: [10.5194/tc-10-1933-2016](https://doi.org/10.5194/tc-10-1933-2016).
- Wagner TJW, James TD, Murray T and Vella D (2016) On the role of buoyant flexure in glacier calving. *Geophysical Research Letters* **43**, 232–240. doi: [10.1002/2015GL067247](https://doi.org/10.1002/2015GL067247).
- Wagner TJW and 6 others (2019) Large spatial variations in the flux balance along the front of a Greenland tidewater glacier. *The Cryosphere* **13**, 911–925. doi: [10.5194/tc-13-911-2019](https://doi.org/10.5194/tc-13-911-2019).
- Warren C, Benn D, Winchester V and Harrison S (2001) Buoyancy-driven lacustrine calving, Glacier Nef, Chilean Patagonia. *Journal of Glaciology* **47**(156), 135–146. doi: [10.3189/172756501781832403](https://doi.org/10.3189/172756501781832403).
- Wood M and 7 others (2018) Ocean-induced melt triggers glacier retreat in northwest Greenland. *Geophysical Research Letters* **45**(16), 8334–8342. doi: [10.1029/2018GL078024](https://doi.org/10.1029/2018GL078024).